

## Synthesis of $\text{Cu}_3\text{SnS}_4$ Nanoparticles with a Novel Structure as Low-Cost Counter Electrode in Dye-Sensitized Solar Cell

Benguang Zhao, Shengping Li, Min Che, Lei Zhu\*

School of Materials Science and Engineering, China University of Mining and Technology, Xuzhou 221116, China

\*E-mail: [lzhu@cumt.edu.cn](mailto:lzhu@cumt.edu.cn)

Received: 7 May 2016 / Accepted: 30 May 2016 / Published: 7 July 2016

---

$\text{Cu}_3\text{SnS}_4$  (CTS) nanoparticles with dendritic structure were synthesized by a facile solvothermal method. The NPs with unique structure are suitable as the precursor of the CE due to their large specific surface area. CTS powder was dispersed in distilled water to form a uniform nanoparticle “ink”. A pure CTS counter electrode for dye-sensitized solar cell (DSSC) was fabricated by coating the CTS “ink” on fluorine-doped tin oxide glass substrate. Electrochemical impedance spectroscopy indicated that CTS-based CE has a Pt-like electrocatalytic activity for the reduction of  $\text{I}_3^-$  to  $\text{I}^-$  in DSSC. DSSC with this novel CE exhibited an impressive power conversion efficiency of 7.13%, which is similar to that Pt/FTO based device (7.24%). This work presents a new approach that using inexpensive CTS replace noble metal Pt as counter electrode for developing low-cost DSSC.

---

**Keywords:**  $\text{Cu}_3\text{SnS}_4$ ; nanoparticle; coating; counter electrode; dye-sensitized solar cell

### 1. INTRODUCTION

Since initially reported by O'Regan and Grätzel in 1991, dye-sensitized solar cell (DSSC) has received extensive attention owing to its low cost and relatively high efficiency.[1-4] Typically, a dissolved  $\text{I}^-/\text{I}_3^-$  redox couple between the electrodes, and a catalytic counter electrode (CE).[5-7] CE is to transfer electrons arriving from the external circuit back to the redox electrolyte and catalyzes the reduction of  $\text{I}_3^-$  ions in electrolyte. A CE usually consists of a thin platinum (Pt) nanoparticle (NP) layer coated on the fluorine doped tin oxide (FTO) glass substrate.[8-11] Nevertheless, this is not an economy way for mass production due to high price of noble metal Pt.[12,13] Some alternatives were investigated to replace Pt as CE in DSSC, such as inorganic materials, carbon materials and conjugated polymers..[14-17]

Recently, Chalcogenides received much attention as CEs due to their excellent electrocatalytic property. Quaternary  $\text{Cu}_2\text{ZnSnS}_4$  (CZTS) NPs have been synthesized and fabricated as CE for DSSC using a spin-coated method by Lin and his coworkers.[18] The CZTS-based CEs exhibited an impressive electrocatalytic performance to promote the regeneration of  $\text{I}^-$  from  $\text{I}_3^-$  in electrolyte. Comparing with quaternary chalcogenide, ternary chalcogenide have simpler composition, in favor of realizing better stoichiometricity.[19-22] Ternary  $\text{Cu}_2\text{SnSe}_3$  has been used as CE for DSSC in our previous work.[23] The  $\text{Cu}_2\text{SnSe}_3$ -based CEs also exhibited an satisfactory electrocatalytic performance and efficiency of the cells base on this CEs reached 3.09%. Because of the similarity of the structure of  $\text{Cu}_3\text{SnS}_4$  to that of  $\text{Cu}_2\text{SnSe}_3$ , The same as  $\text{Cu}_2\text{SnSe}_3$ ,  $\text{Cu}_3\text{SnS}_4$  also belongs to the family of chalcogenide comprising only three kind of elements. However, there were still few reports on the application of  $\text{Cu}_3\text{SnS}_4$  as CE. Therefore, we have been motivated to develop  $\text{Cu}_3\text{SnS}_4$  as efficient C in DSSC.

In this study, CTS NPs were synthesized by solvothermal method then dissolved in distilled water to form uniform “ink”. A pure CTS counter electrode was fabricated by coating the  $\text{Cu}_3\text{SnS}_4$  “ink” as precursor on FTO glass substrate. The effect of the CTS film thickness on electrocatalytic activity and photovoltaic performance was also investigated. Due to its simplicity, low cost, and large scalability, there is potential for the use of CTS NPs as a CE to obtain a high-performance DSSC.

## 2. EXPERIMENTAL DETAILS

### 2.1 Synthesis of CTS NPs and preparation of electrodes for DSSCs

CTS NPs were synthesized by a typical solvothermal method as we reported before. In briefly, Copper (II) sulfate (1.5 mmol, 99%, Aladdin), Stannic chloride hydrated (0.5 mmol, 99%, Aladdin) and S (2 mmol, 99.99%, Aladdin) were dissolved in distilled water (25 mL) under stirring, then ethylenediamine monohydrate (50 mL, 98%) was added and magnetically stirred for 20 min, then the solution was transferred into a 100 mL stainless steel Teflon-lined autoclave. The autoclave was sealed and the mixture temperature was kept at 200 °C for 25 h, the autoclave was cooled to room temperature naturally. The mixture was then diluted with deionized water and precipitated with absolute ethylalcohol. The product were separated by centrifugation at 5000  $\text{r}\cdot\text{min}^{-1}$  for 5 min and the byproduct was decanted, then the precipitate was dispersed again in deionized water. The alternating precipitation and dispersion process was repeated for several times. The final dark product was collected after being vacuum-dried at 60 °C for 12 h. The CTS NPs were dissolved in distilled water concentrated to 150  $\text{mg}\cdot\text{mol}^{-1}$  and ultrasonicated for 20 min to form uniform “ink”. The “ink” was coated on to a thoroughgoing cleaned FTO substrate by a drop-casting method. The drop-casting area was controlled to be 0.8 cm $\times$  0.8 cm and the thickness of CTS films was adjusted by the drop volume of “ink” with 0.1, 0.2, 0.3 and 0.4 mL. The films were vacuum-dried fully at room temperature for 25 h and subsequently annealed at 550 °C for 35 min in sulfur vapor to obtain CTS thin films as CEs. Pt-coated FTO glass was prepared by adopting a dipping-pulling method to coat the 5  $\text{mg}\cdot\text{mol}^{-1}$   $\text{H}_2\text{PtO}_6$

on the FTO glass and sintered at 390 °C for 20 min as Pt CE. TiO<sub>2</sub> NPs (P25, Degussa) were prepared by mixing 1 g P25, 2 mL distilled water, 0.3 g PEG 20000, 3 drop of Triton X-100 in an agate mortar. Then, the mixture was grinded for 4 hours. TiO<sub>2</sub> NPs layer was spin coated on the FTO glass. After sintering at 500 °C for 3 h and cooling down to 80 °C, the TiO<sub>2</sub> NPs-coated FTO glass was immersed into TiCl<sub>4</sub> aqueous solution and kept in an oil bath at 70 °C for 1 h and sensitized in a 3 mg·mol<sup>-1</sup> N719 ethanol solution for 24 h.[24]

## 2.2. Assembly of DSSCs

The solar cell was assembled in a typical sandwich-type cell by placing an as-prepared CTS-coated or Pt-coated FTO conducting glass on the dye-sensitized TiO<sub>2</sub> photoanode. CE is separated from photoanode by applying a 60 μm thick thermal-plastic surlyn (DHS- SN1760) as the spacer then the assembled DSSC was clipped together and heated to 100 °C for 10 min for encapsulation. The redox electrolyte used in this study was an ionic liquid containing 0.50 g·mol<sup>-1</sup> 4-tert-butylpyridine in the mixture of acetonitrile and valeronitrile (volume ratio: 85:15). A commercially available ionic electrolyte solution (Dalian Hepta Chroma) was injected between two electrodes through the holes of the CE. Finally, the holes were blocked with the melting thermal-plastic surlyn which rewarmed by electric soldering iron and cooling down to room temperature naturally.

## 2.3. Structural, morphological and photoelectrical characterization

The morphologies, crystal structure and chemical constitution of the CTS were characterized by field-emission scanning electron microscope (FESEM, Hitachi S-4800, Japan), transmission electron microscopy (TEM, Jeol-2010, Japan) and X-ray diffraction (XRD, Bruker D8 Advance, Germany). The photocurrent density-voltage (J-V) measurements were carried out under illumination of 100 mW·cm<sup>-2</sup> using a Keithley model 2420 digital source meter. A solar simulator was used to simulate sunlight by a 500 W xenon lamp light source fitted with an AM1.5G filter (Beijing Trusttech). The illumination intensity of 100 mW·cm<sup>-2</sup> was calibrated with a standard monocrystalline silicon solar cell which passed the American Society for Testing and Materials (ASTM) calibration. Electrochemical impedance spectroscopy (EIS) analysis was conducted by using electrochemical test station (CHI660D) under illumination 100 mW·cm<sup>-2</sup>.

## 3. RESULTS AND DISCUSSION

The morphology and structure of CTS NPs were showed in Fig. 1 with various magnifications. The shape of CTS NPs is dendritic structure with the size of 200-300 nm. Fig. 1(b) is a high-magnification FESEM micrograph of CTS NPs, it can be seen that the dendritic structure NPs are composed of many tiny interconnected nanocrystal and its surfaces are considerably rough. Note that, the NPs with this peculiar dendritic structure is top suitable as CE for DSSC. First, the branch structure

and its coarse surface can increase the specific surface area which is beneficial for increasing the number of the catalytic site. Second, CTS films containing dendritic structure NPs have enough internal space for increasing contact area between CE and electrolyte. Last, the interconnected nanocrystal can provide a pathway for electron transfer. Fig. 1(c) displays the TEM images of CTS NPs, the diameters of the NPs are about 250 nm, which are in accordance with the FESEM results. Some of the tiny nanocrystals with the size of about 20 nm can be seen from the edge of some NPs. The lattice fringe of 0.32 nm (Fig. 1d) matches the spacing distance of (112) plane and agrees well with that determined from the diffraction peak at  $28.49^\circ$  in XRD pattern. The cross-sectional FESEM images of the CTSe thin film after annealing are presented in Figure. 2(a-d), increasing the drop volume (0.1, 0.2, 0.3 and 0.4 mL) gives rise to an increase in film thickness, 2.1, 2.9, 3.3 and 4.8  $\mu\text{m}$ , respectively.

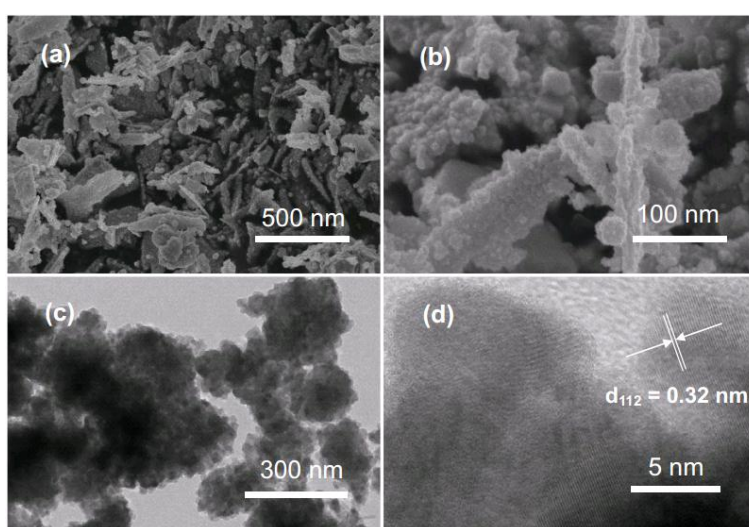


**Figure 1.** FESEM images of as-obtained CTS NPs with (a) low and (b) high magnifications. (c) TEM image and (d) HRTEM image of the as-obtained CTS NPs.

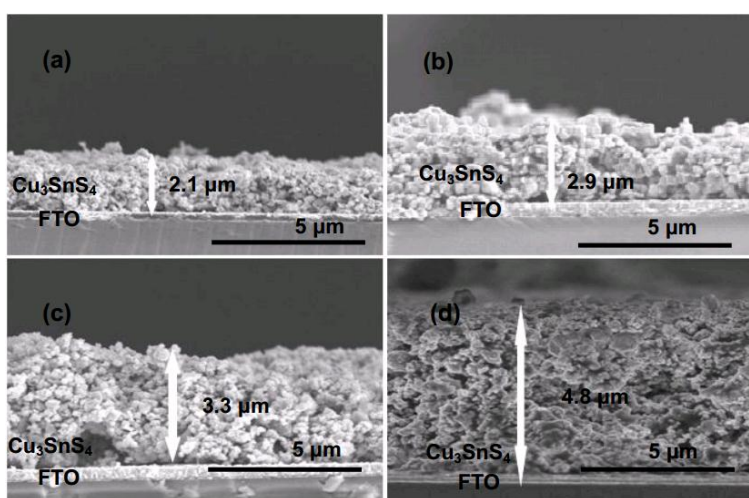


**Figure 2.** Cross-sectional FESEM images of CTS thin film with drop volume of (a) 0.1, (b) 0.2, (c) 0.3, and (d) 0.4 mL.

Fig. 3 shows a typical XRD pattern of the annealed CTS NPs. The major XRD diffraction peaks appeared at  $2\theta = 28.49^\circ$ ,  $47.46^\circ$ ,  $56.02^\circ$ ,  $69.82^\circ$  and  $76.52^\circ$ , which could be attributed to (112), (220), (132), (008) and (332) planes, respectively. All the diffraction peaks could be assigned to the crystal planes from standard cubic structure CTS without any other peaks being observed (JCPDS Card, No.33-0501). It is illuminated that the CTS NPs were pure without any other phase. All of the peaks were acute, suggesting that the films were crystallized well after annealing. On the basis of the XRD pattern, CZTS has the following crystal structures:  $I-42m$  cubic structure ( $a=5.445\text{\AA}$ ), which was accordance with the data reported by the previous reports.[25]

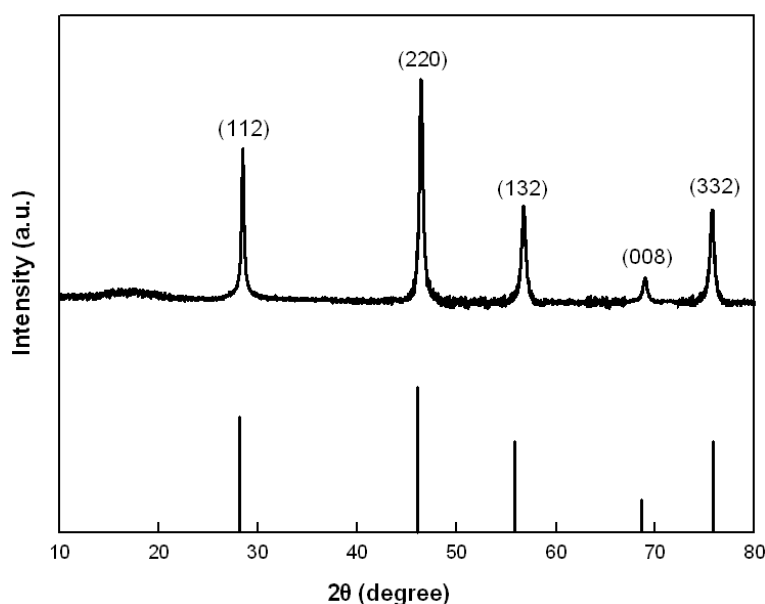


**Figure 3.** XRD pattern of CTS NPs after annealing

Fig. 4 shows the current–voltage curves of DSSCs fabricated with Pt and different thickness CTS-based CEs. The corresponding photovoltaic parameters were summarized in Table. 1, including the short-current density ( $J_{sc}$ ), the open-circuit voltage ( $V_{oc}$ ), the fill factor (FF) and the power conversion efficiency ( $\eta$ ). When the drop volume was 0.2 mL, a highest efficiency of  $\eta = 7.13\%$  was achieved with  $J_{sc} = 13.51 \text{ mA}\cdot\text{cm}^{-2}$ ,  $V_{oc} = 0.71 \text{ V}$  and  $FF = 72.93\%$ . It is clear that the photocurrent density first increases from  $12.32$  to  $13.51 \text{ mA}\cdot\text{cm}^{-2}$  with increasing the thickness of the thin film from  $2.2 \mu\text{m}$  (drop volume 0.1 mL) to  $2.9 \mu\text{m}$  (0.2 mL). However, while further increasing the thickness of the film to  $3.3 \mu\text{m}$  and  $4.8 \mu\text{m}$ , the photocurrent density decreases significantly to  $11.21$  and  $10.30 \text{ mA}\cdot\text{cm}^{-2}$ , respectively. This may be due to the value of  $J_{sc}$  is influenced by the number of the electrocatalytic sites and different resistance in films with dissimilar thickness. There are more electrocatalytic sites in thicker films would be beneficial to the electrocatalytic activity meanwhile larger resistance would be harmful for charge transport which is caused by more abundant grain boundaries and defects. When the thickness reached  $2.9 \mu\text{m}$ , we got a satisfactory result due to the synergic effects of the amount of electrocatalytic sites and the value of resistance. The FF increases from  $71.87\%$  to  $75.12\%$  with the increase of the film thickness. This is due to the CTS film is

composed of small interconnected nanocrystals and interspace. With the increase in the film thickness, CTS film has more contact area with electrolyte. Hence, thicker CTS-based CE can provides relatively larger amount of electrocatalytic sites which is beneficial to the electrocatalytic activity and leads to the increase of the FF.

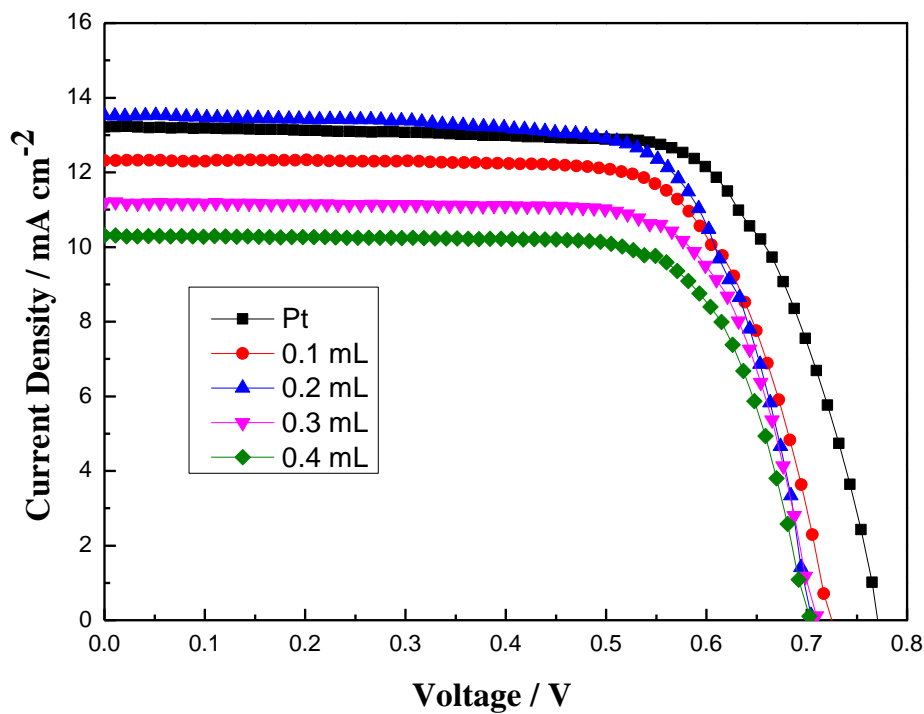


**Figure 4.** Current-voltage characteristics of DSSCs with Pt and different thickness CTS CEs under AM1.5 sunlight illumination of  $100\text{mW}\cdot\text{cm}^{-2}$

EIS measurement was performed to further clarify the photovoltaic behavior of the CE. The Nyquist plots and the equivalent circuit were shown in Fig. 5. The high frequency (corresponding to low  $Z'$ ) intercept on the real axis ( $Z'$  axis) represents the series resistance  $R_s$ , The semicircle in the high-frequency range results from the charge-transfer resistance ( $R_{ct}$ ) and the corresponding constant phase-angle element (CPE) at the electrolyte/CE interface.[26,27] The values of  $R_s$ ,  $R_{ct}$  obtained by fitting the spectra in Fig. 5 with an EIS spectrum analyzer are summarized in Table 1. The  $R_s$  of CTS-based CEs were larger than that of the Pt-based CE, which was most likely due to the relatively large conductivity of Pt comparing with semiconductor CTSe.  $R_s$  is increased while increasing CTS-based CEs thickness. This is due to the distance of electron transport increased in a thicker CE. The  $R_{ct}$  of all CTS-based CEs were less than that of Pt-based CE, indicating a superior catalytic property of CTS. The  $R_{ct}$  is decreased as increase the thickness of CTS thin film. It is illustrated that thicker film has a better catalytic activity which may be due to more electrocatalytic sites can be provide. The EIS results agreed well with the current–voltage curve. It suggested that the CTS was excellent to be a candidate for replacing Pt as CE in DSSC.

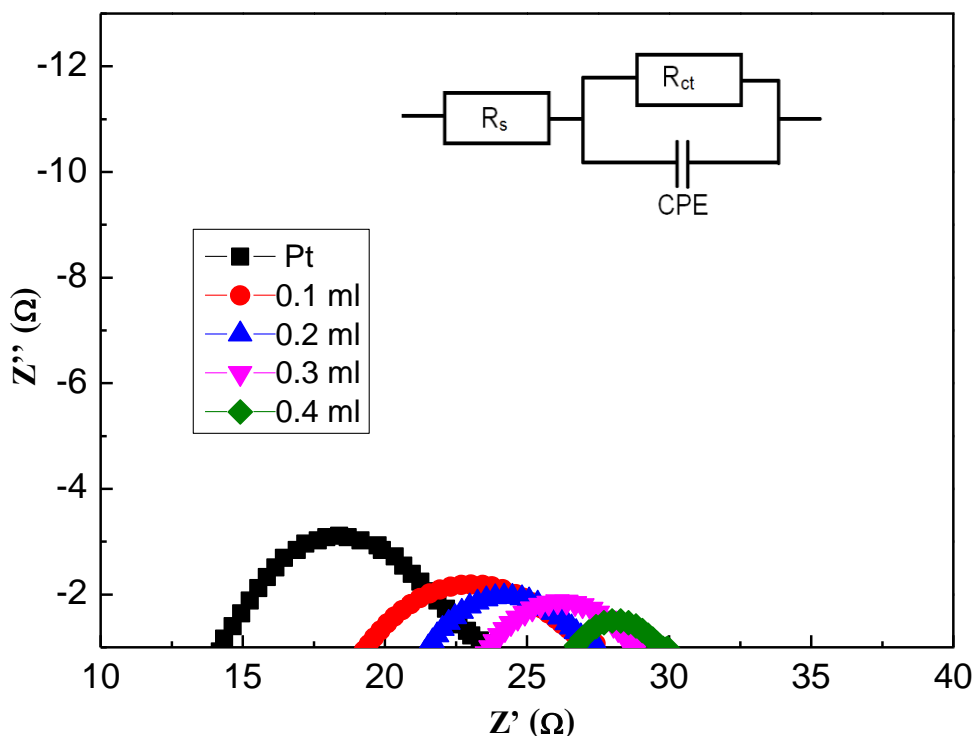


**Figure 5.** Nyquist plots of the DSSCs with Pt and different thickness CTS CEs from EIS under

AM1.5 sunlight illumination of  $100 \text{ mW cm}^{-2}$ . The inset indicates an equivalent circuit used for fitting the EIS results, including the series resistance ( $R_s$ ), charge-transfer resistance ( $R_{ct}$ ) and constant phase-angle element (CPE).

**Table 1.** Series resistance ( $R_s$ ), electron transfer resistance ( $R_{ct}$ ), short-current density ( $J_{sc}$ ), the open-circuit voltage ( $V_{oc}$ ), the fill factor (FF) and the power conversion efficiency ( $\eta$ ) of DSSCs fabricated with Pt and different thickness CTS CEs under AM1.5 sunlight illumination of  $100 \text{ mW}\cdot\text{cm}^{-2}$ .

Drop volume /mL	Thickness / $\mu\text{m}$	$R_s / \Omega$	$R_{ct} / \Omega$	$J_{sc} / \text{mA}\cdot\text{cm}^{-2}$	$V_{oc} / \text{V}$	FF/%	$\eta / \%$
Pt	0.5	13.52	10.57	13.16	0.77	71.36	7.24
0.1	2.2	18.67	7.34	12.32	0.73	71.87	6.47
0.2	2.9	21.34	5.48	13.51	0.71	72.93	7.13
0.3	3.3	23.28	4.51	11.21	0.71	73.82	5.89
0.4	4.8	26.31	3.52	10.30	0.69	75.12	5.35

#### 4. CONCLUSION

We successfully synthesized the pure CTS NPs with the size of 200-300 nm by a facile solvothermal method. The NPs with unique dendritic structure are suitable as the precursor of the CE due to their large specific surface area. A new structure CTS-based CE was fabricated via a drop-

casting method for DSSC. EIS measurement indicated that CTS-based CE exhibited Pt-like electrocatalytic activity for the reduction of  $\Gamma/I_3^-$  in DSSCs. Photocurrent density and fill factor of the solar cell was affected by the thickness of the film remarkably. The obtained cell based on low-cost CTS as CE exhibited a optimal power conversion efficiency of 7.13%, which was similar to those conventional Pt-based ones (7.24%). Considering its great cost advantage, CTS as a candidate is very promising to replace Pt as CE in DSSC. Further work will be focused on the improvement of the energy conversion efficiency by optimizing the parameters, such as the film annealing temperature, assembly technology of the solar cells.

#### ACKNOWLEDGEMENTS

This work was financially supported by the Fundamental Research Funds for the Central Universities (2015QNA09).

#### References

1. B. O'Regan, and M. Grätzel, *Nature*, 353 (1991) 737-740.
2. J. Yu, J. Fan, and C. Bei, *Journal of Power Sources*, 196 (2011) 7891-7898.
3. M. Gratzel, *Nature*, 414 (2001) 338-344.
4. B. T. Xiong, B. X. Zhou, J. Bai, Q. Zheng, Y. B. Liu, W. M. Cai and J. Cai, *Chinese Physics B*, 17 (2008) 3713-3719.
5. Mori S, Sunahara K, Fukai Y, Kanzaki T, Wada Y and Yanagida, *Journal of Physical Chemistry C*, 112 (2008) 20505-20509.
6. H. J. Snaith, *Advanced Functional Materials*, 20 (2010) 13-19.
7. G. R. Li, F. Wang, Q. W. Jiang, X. P. Gao, P. W. Shen, *Angewandte Chemie*, 49 (2010):3653-6.
8. P. J. Li, K. Chen, Y. F. Chen, Z. G. Wang, X. Hao, J. B. Liu, J. R. He and W. L. Zhang, *Chinese Physics B*, 21 (2012) 490-494.
9. J. Luo, H. J. Niu, W. J. Wu, C. Wang, X. D. Bai and W. Wang, *Solid State Sciences*, 48 (2013) 145-149.
10. V. D. Dao, S. H. Ko, H. S. Choi, J. K. Lee, *Journal of Materials Chemistry*, 22 (2012) 14023-14029.
11. Luo Y, Li D and Meng Q, *Advanced Materials*, 21 (2009) 4647-4651.
12. Q. Li, Z. G. Cheng, Li Z. G., Wang Z H and Fang Y, *Journal of Applied Physics*, 107 (2010) 12-15.
13. X. Q. Dai, Y. N. Tang, Y. W. Dai, Y. H. Li, J. H. Zhao, B. Zhao and Z. X. Yang, *Chin. Phys. B*, 20 (2011) 335-341.
14. K. Miettunen, M. Toivola, G. Hashmi, J. Salpakari, I Asghar, P. Lund, *Carbon*, 49 (2011) 528-532.
15. S. U. Lee, W. S. Choi and B. Hong, *Solar Energy Materials & Solar Cells*, 94 (2010) 680-685.
16. G. Zhu, L. Pan, T. Lu, X. J. Liu, T. Lv, T. Xu and Z. Sun, *Journal of Materials Chemistry*, 56 (2011) 10288-10291.
17. J. D. Roy-Mayhew, I. A. Aksay, *Chemical Reviews*, 114 (2014) 6323-6348.
18. X. K. Xin, M. He, W. Han, J. Jung and Z. Q. Lin, *Angewandte Chemie*, 50 (2011) 11739 - 11742.
19. S. Bag, O. Gunawan, T. Gokmen, Y. Zhu, T. K. Todorov and D. B. Mitzi, *Energy & Environmental Science*, 5 (2012) 7060-7065.
20. Y. Yang, Y.H. Qiang, J. Song, Z. Xing, C. B. Song, *International Journal of Electrochemical Science*, 10 (2015) 5479-5487.
21. A. Walsh, S. Chen, S. H. Wei, X. G. Gong, *Advanced Energy Materials*, 2 (2012) 400-409.

22. C. B. Song, Y. L. Zhao, D. M. Sogn, L. Zhu, X. Q. Gu, & Y. H. Qiang, *International Journal of Electrochemical Science*, 9 (2014) 3158-3165.
23. G. Marcano, C. Rincón, L. M. de Chalbaud, D. B. Bracho, G. Sánchez Pérez, *Journal of Applied Physics*, 90 (2001) 1847-1853.
24. X. P. Lin, D. M. Song, X. Q. Gu, Y. L. Zhao and Y. H. Qiang, *Applied Surface Science*, 263 (2012) 816-820.
25. Y. F. Du, J. Q. Fan, W. H. Zhou, Z. J. Zhou, J. Jiao and S. X. Wu, *Acs Applied Materials & Interfaces*, 4 (2012) 1796-802.
26. T. W. Hamann, R. A. Jensen, A. B. F. Martinson, H. V. Ryswyk and J. T. Hupp, *Energy & Environmental Science*, 1 (2008) 66-78.
27. M. Yanagida, *Advances in Natural Sciences Nanoscience & Nanotechnology*, 6 (2015).

© 2016 The Authors. Published by ESG ([www.electrochemsci.org](http://www.electrochemsci.org)). This article is an open access article distributed under the terms and conditions of the Creative Commons Attribution license (<http://creativecommons.org/licenses/by/4.0/>).